

# Revisiting the structure of UBR box from human UBR6

Bokyung Kim | Sohae Lee | Bong Heon Kim | Leehyeon Kim |  
 Hyun Kyu Song 

Department of Life Sciences, Korea University, Seoul, South Korea

#### Correspondence

Hyun Kyu Song, Department of Life Sciences, Korea University, 145 Anam-ro, Seongbuk-gu, Seoul 02841, South Korea.  
 Email: [hksong@korea.ac.kr](mailto:hksong@korea.ac.kr)

#### Present addresses

Bokyung Kim, Department of Integrative Structural and Computational Biology, The Scripps Research Institute and Howard Hughes Medical Institute, La Jolla, California, USA; and Leehyeon Kim, Cell Biology Program, Sloan Kettering Institute, Memorial Sloan Kettering Cancer Center, New York, New York, USA.

#### Funding information

National Research Foundation of Korea, Grant/Award Numbers: RS-2020-NR049540, RS-2021-NR056525, RS-2021-NR056577, RS-2022-NR067411; Korea University

Review Editor: Margaret Shun Cheung

## Abstract

Eukaryotic N-degron pathways are proteolytic systems with the ability to recognize specific N-terminal residues of substrate proteins, which are essential parts of their degradation signals. Domains, referred to as UBR boxes, of several E3 ubiquitin ligases can recognize basic N-terminal residues as N-degrons. UBR6 is among the seven mammalian UBR family proteins containing the UBR box domain. However, the recognition of basic type-1 N-degrons by UBR6 is still not well understood. The crystal structure of the UBR box from human UBR6 revealed zinc-mediated dimerization, a structural feature distinct from other monomeric UBR boxes. Furthermore, its folding pattern differed from that of the UBR fold, although the sequences aligned well with those of other UBR boxes. In this study, we re-determined the structure of the UBR box from human UBR6 to investigate whether the unusual domain-swapped dimer was structurally relevant. The newly determined UBR box of UBR6 at 1.5 Å resolution was a monomer with a classical UBR fold. Our structure was compared with previously reported structures of UBR boxes, and its structural features were further analyzed using N-degron binding assays.

## KEY WORDS

AlphaFold, crystal structure, FBXO11, N-degron pathway, N-end rule, UBR6, X-ray crystallography

## 1 | INTRODUCTION

The N-degron pathway (formerly the N-end rule) is a branch of the ubiquitin-proteasome system, a process that controls the half-life of proteins based on the N-terminal residue called N-degron (Bachmair et al. 1986; Varshavsky 1996, 2011, 2019). N-degrons are classified into two types depending on the characteristics of the residues: type-1 N-degrons (positively charged residues: Arg, Lys, and His) and type-2 N-degrons (bulky hydrophobic residues: Leu, Phe, Tyr, Trp, and Ile). They are selectively recognized by N-recognin, an E3 ubiquitin ligase that recognizes N-degrons (Bartel et al. 1990; Pan et al. 2021). Ubr1 N-recognin from *Saccharomyces cerevisiae* was the first E3 enzyme to be characterized among more than 600 E3 ubiquitin ligases (Bartel et al. 1990), and UBR1 and UBR2 are mammalian homologs. They possess a

UBR box domain for type-1 substrates and a ClpS-homology domain for type-2 substrates (Choi et al. 2010; Kim et al. 2021; Pan et al. 2021; Tasaki et al. 2005; Varshavsky 1996, 2011, 2019). The substrate bound to the N-recognin is ubiquitylated and ultimately degraded by the 26S proteasome (Finley 2009; Schrader et al. 2009; Tasaki et al. 2012; Varshavsky 2024).

The UBR box is a zinc finger domain in the UBR family of E3 ubiquitin ligases, and there are seven UBR proteins encoded in the mammalian genome (Tasaki et al. 2005; Tasaki and Kwon 2007). Among these, UBR1, UBR2, UBR4, and UBR5 are N-recognins that bind to type-1 N-degrons of substrates through their UBR box (Hodakova et al. 2023; Sriram et al. 2011; Tasaki et al. 2005; Tsai et al. 2023; Wang et al. 2023). Intriguingly, other UBR proteins, including UBR3, UBR6, and UBR7, possess a UBR box domain, but it is unclear whether they act as N-recognins (Tasaki et al. 2009). The N-degron binding mode of the

Bokyung Kim and Sohae Lee contributed equally to this study.

UBR box has been well-established in extensive structural studies (Choi et al. 2010; Kim et al. 2020; Kim et al. 2023; Matta-Camacho et al. 2010; Munoz-Escobar et al. 2017b). However, the structure of the UBR box for nonfunctional UBR-containing N-recognins is not well understood.

UBR6, also known as FBXO11, is an F-box protein in the Skp1-Cullin-F-box (SCF) ubiquitin ligase complex (Jackson and Eldridge 2002; Kipreos and Pagano 2000; Skaar et al. 2013). The SCF complex plays an essential role in the terminal differentiation of germinal center B-cells toward memory B-cells and plasma cells by targeting BCL6. It also regulates TGF- $\beta$  signaling, cell migration, and the timing of cell-cycle progression by targeting DTL/CDT2 (Abbas et al. 2013a, 2013b; Abida et al. 2007; Duan et al. 2012; Horn et al. 2014; Rossi et al. 2013). As an F-box protein, UBR6/FBXO11 directly binds to target proteins; however, its substrate-binding mechanism remains unknown. Although UBR6 contains a C-terminal UBR box domain, it does not bind to N-degrons. Instead, two carbohydrate-binding/sugar hydrolysis (CASH) domains or parallel beta-helix repeats (PbH1) between the N-terminal F-box domain and the C-terminal UBR box domain have been reported as substrate-binding sites (Duan et al. 2012; Jin et al. 2004) (Figure S1, Supporting Information).

Notably, a domain-swapped dimer structure of the UBR box of human UBR6 (hUBR6) has been reported (Munoz-Escobar et al. 2017). The results showed that the UBR box from hUBR6 (UBR6-box<sup>833–904</sup>) is a dimer in solution and resembles a typical UBR box structure formed by the domain swapping of two monomers. However, this seems to be an unusual domain swapping mediated by zinc atoms because the sequence of the UBR6-box does not differ greatly among all other UBR family proteins (Choi et al. 2010; Kim et al. 2020; Matta-Camacho et al. 2010; Munoz-Escobar et al. 2017; Tasaki et al. 2005). Therefore, we investigated the structure of the UBR6-box using different constructs to determine whether the domain-swapped dimer was structurally relevant. We found that the N-terminally extended construct of the UBR6-box (UBR6-box<sup>824–908</sup>) was a monomer in solution, and we determined its high-resolution structure. We also compared the structural features of the UBR6-box<sup>824–908</sup> with previously known structures of UBR boxes from UBR1, UBR2, and UBR6 and subsequently analyzed their ability to bind to the N-degron substrate using biochemical results.

## 2 | RESULTS

### 2.1 | The N-terminal-extended UBR box from hUBR6 is a monomer in solution

The reported domain-swapped structure comprises residues 833–904 of hUBR6 (Munoz-Escobar et al. 2017).

The most characteristic feature of this structure was dimerization by His<sub>4</sub>-zinc coordination, which is an uncommon coordination. Therefore, we tested various constructs, such as the different lengths of the N- and C-terminal extensions of the previous 833–904 version. The oligomeric states of a more extended C-terminal construct (residues 833–908) showed a significant fraction of dimeric species and varied primarily in terms of the Zn(II) ion concentration during protein production (Figure S2). When the N-terminal-extended construct of UBR6-box (residues 824–908) was predicted with AlphaFold (Abramson et al. 2024; Jumper et al. 2021), the model was a monomer with one more N-terminal  $\alpha$ -helix, but not a dimer (Figure S3a). The predicted structure of UBR6-box<sup>824–908</sup> showed different conformations of the N-terminal helix depending on the presence of zinc atoms (Figure S3a), and the prediction of the entire UBR6 showed a monomeric structure with a monomeric UBR box (Figure S1b). The previously determined dimeric UBR6-box<sup>833–904</sup> exhibited a steric clash upon superimposition with the entire UBR6 (Figure S3b).

Experimentally, UBR6-box<sup>824–908</sup> was eluted as a sharp peak in ion exchange chromatography and was predominantly eluted at the monomer peak position in size-exclusion chromatography (Figure 1a,b). To confirm the oligomeric state of the UBR box<sup>824–908</sup>, we performed size-exclusion chromatography coupled with multi-angle light scattering (SEC-MALS) and verified that most of the proteins existed as monomers (Figure 1c). The experimentally determined molecular mass of the small dimer peak eluted earlier was 23.5 kDa (calculated as 20.0 kDa). The molecular mass of the monomer showed a main peak at 12.8 kDa (calculated as 10.0 kDa). The 824–908 construct yielded approximately 7 mg per 1 L of culture, with over 99% final purity, which is at least seven times higher than that of the other constructs. Therefore, the hUBR6-box<sup>824–908</sup> construct with an extended N-terminal region was predominantly in a more stable monomeric state.

### 2.2 | Crystal structure of UBR6-box from hUBR6

Crystals of the UBR6-box<sup>824–908</sup> were obtained using a 12 mg/mL concentration, and the best-shaped crystal was diffracted to a 1.5 Å resolution. The structure of the zinc atoms was determined using multi-wavelength anomalous dispersions (MAD). The data collection and refinement statistics are presented in Table S1. One monomeric UBR6-box<sup>824–908</sup> molecule was in the asymmetric unit, and the monomer was composed of four  $\alpha$ -helices and two  $\beta$ -sheets, similar to the known UBR fold (Figure 2a). The zinc-coordinating residues of UBR6 were well conserved among all UBR proteins

**FIGURE 1** Purification and molecular mass determination of the target protein. (a) Ion exchange chromatography profile using Q HP columns. The protein was eluted with a linear NaCl gradient (green line), and absorbance was monitored at 280 nm (blue line). The SDS-PAGE analysis of the eluted fractions is shown on the right. (b) Size-exclusion chromatography profile obtained using a Superdex 75 prep-grade column. The elution profile is depicted in blue, with the corresponding SDS-PAGE analysis of the eluted fractions on the right. (c) SEC-MALS results of UBR6-box<sup>824–908</sup> showing the molecular mass (MM) of the monomer (kDa). The horizontal line represents the measured molecular mass, which is indicated by an arrow with the experimental (MALS) molecular mass and theoretically calculated (Calc) values in parentheses (MALS/Calc).

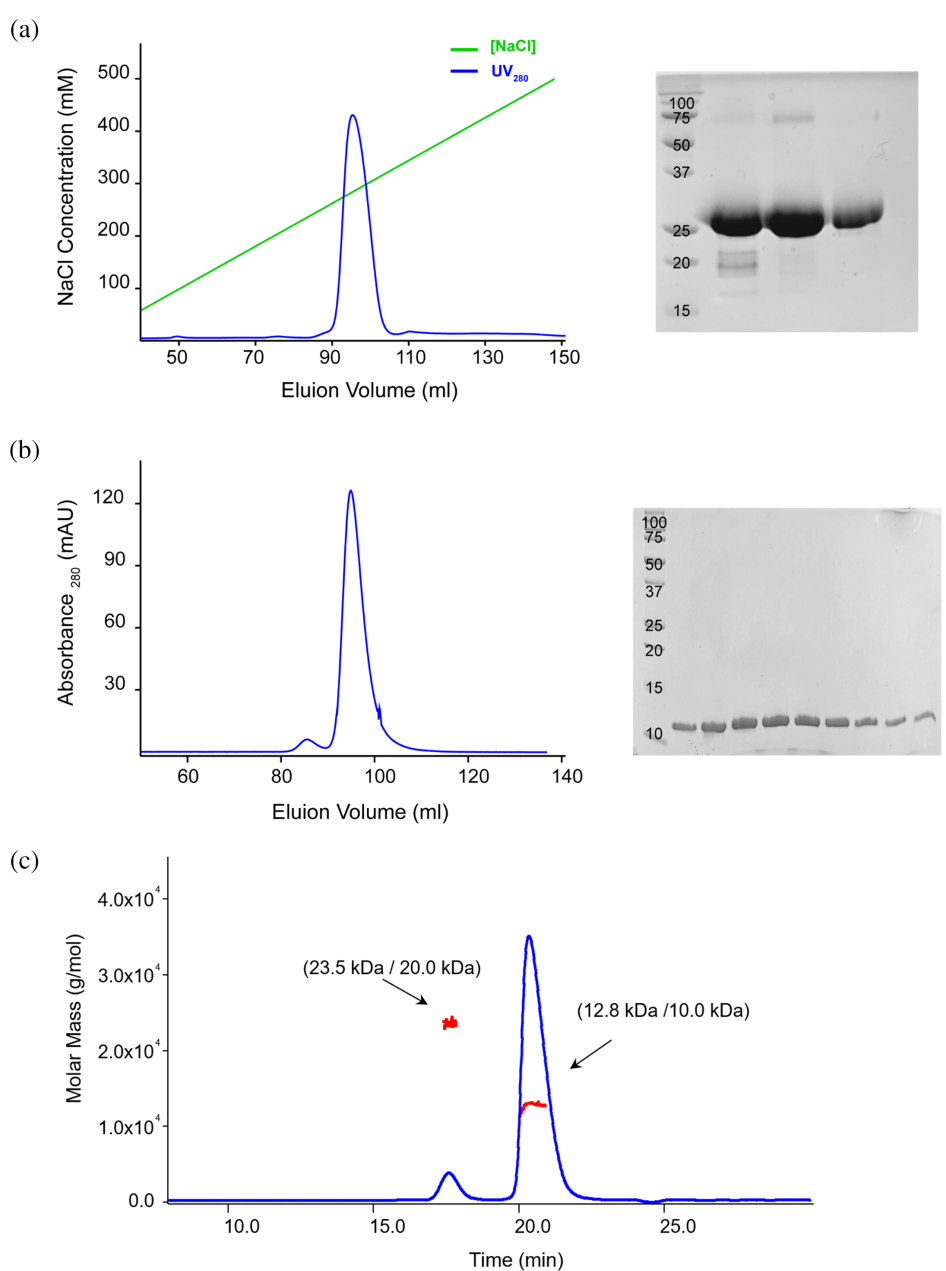


(Figure 2b). One of the unique zinc geometries in the UBR fold was a cysteine residue (Cys868) bridging two zinc atoms (Zn1 and Zn2), which was first described for yUBR1 and hUBR1/2 (Choi et al. 2010; Matta-Camacho et al. 2010) (Figure 2c). Seven residues of hUBR1, hUBR2, and yUBR1 coordinated two zinc ions by a shared cysteine with Cys<sub>3</sub> for the first zinc (Zn1) and with Cys<sub>2</sub>-His for the second zinc (Zn2), resulting in tetrahedral coordination (Choi et al. 2010; Matta-Camacho et al. 2010) (Figure S4). Histidine was replaced by Cys872 in hUBR6, making Cys<sub>4</sub> coordinate with one shared cysteine for the second zinc ion (Figure 2c). The other zinc ion (Zn3) was coordinated by Cys<sub>2</sub>-His<sub>2</sub> in hUBR6, as shown for the other three UBR family proteins (Figure 2b).

### 2.3 | Comparison of monomeric UBR box with the domain-swapped dimer from UBR6

Next, the monomeric structure of hUBR6-box<sup>824–908</sup> was compared with that of a previously determined domain-swapped dimer (Muñoz-Escobar et al. 2017). The structural boundary, composed of two separate polypeptide chains of the domain-swapped UBR6-box<sup>833–904</sup>, showed a folding pattern similar to that of the UBR box (Muñoz-Escobar et al., 2017) (Figure 2d). It also exhibited folding similar to the monomeric UBR6-box structure identified in our current study, but there were differences in the details. The largest difference in the structure was located on

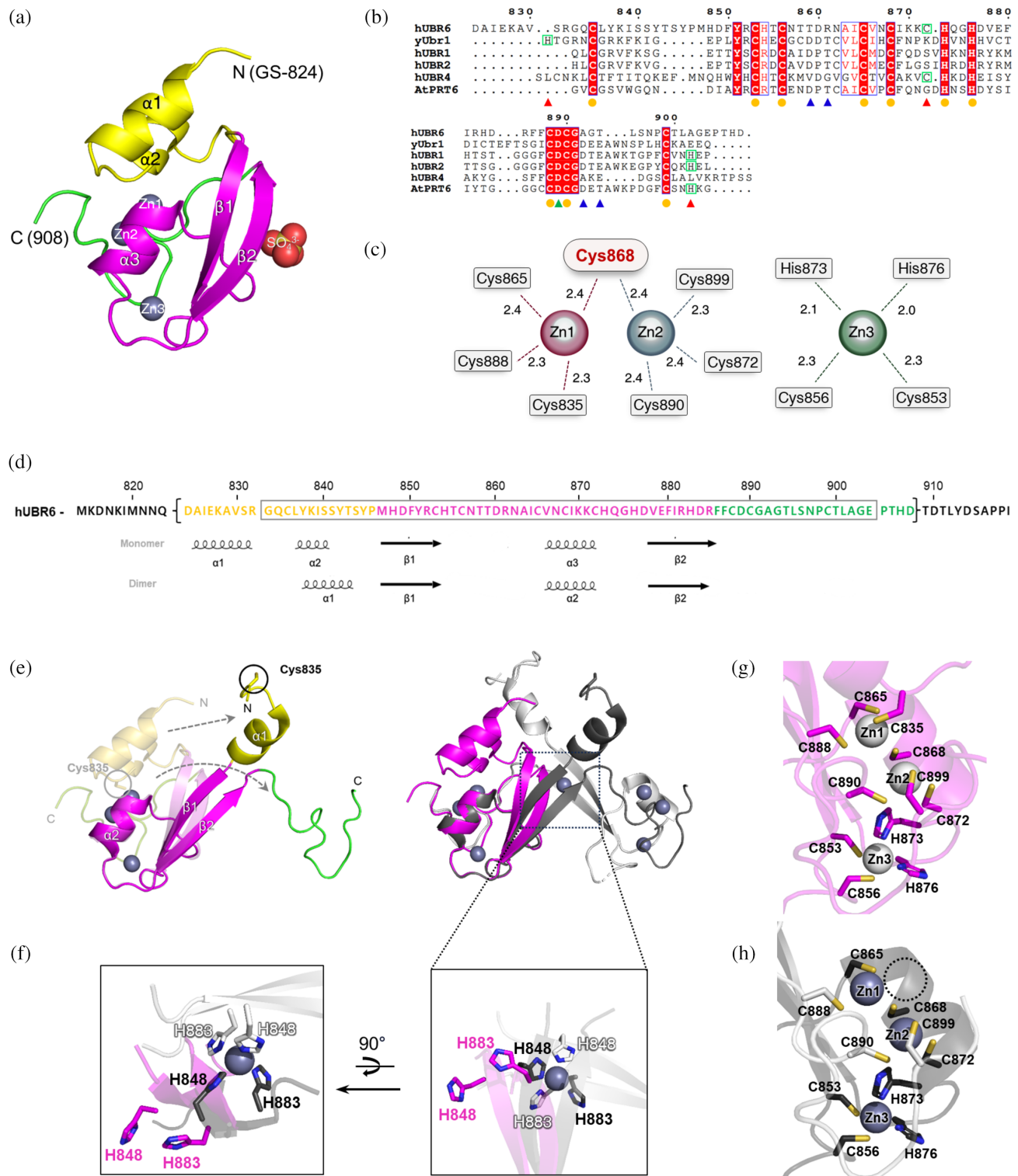


**FIGURE 2** Legend on next page.

the N-terminal region because the hUBR6 824–908 construct had nine more residues forming the first helix  $\alpha$ 1 (Figure 2a). The monomeric hUBR6-box<sup>824–908</sup> had two small N-terminal  $\alpha$ -helices before the  $\beta$ -strand appeared, but the monomer chain of the domain-swapped structure had only one  $\alpha$ -helix in the N-terminus (Figure 2d,e). While hUBR6-box<sup>824–908</sup> had a compact shape, the monomer chain of the domain-swapped structure had an extended shape, where the two  $\alpha$ -helices from each chain were located at the other termini of the  $\beta$ -strands (Figure 2e). The compact structure of the monomer showed a difference in the bending of two  $\beta$ -strands,  $\beta$ 1 and  $\beta$ 2, which formed a zinc-mediated dimerization (Figure 2e,f). The deviated bending was mainly caused by the missing zinc-coordination of Cys835 in the domain-swapped dimer (Figure 2e).

The histidine residues (His848 and His883) that chelated the Zn(II) ion in the separate monomers in the domain-swapped dimer were not involved in metal coordination in monomeric UBR6 and were located within the interior of the molecule (Figure 2e,f). The domain-swapped dimer structure was coordinated with seven zinc ions, with one additional zinc ion in the center for dimerization (Figure 2f). The six zinc ions were coordinated into two sets, each comprising three zinc ions. In each set, zinc ions were coordinated by residues from both peptide chains of the domain-swapped dimer. Remarkably, the three zinc coordination topologies of the dimeric structure were nearly identical to those of the monomeric structure (Figure 2g,h). The first zinc ion was coordinated by Cys835, Cys865, Cys868, and Cys888. Cys868 also coordinated the second zinc ion with Cys872, Cys890, and Cys899. The last zinc ion was coordinated by Cys853, Cys856, His873, and His876. In the domain-swapped dimer structure, the last three cysteine residues (Cys888, Cys890, and Cys899) belonged to different chains.

Cys835 of the domain-swapped structure was not illustrated in Figure 2h because this residue was not on either chain of the dimer but on another adjacent chain within the crystal.

## 2.4 | Comparison with functional UBR boxes

The zinc-coordinating residues of UBR6 were highly conserved among UBR proteins (Figure 2b), and the folding of the monomeric UBR6-box was similar to that of the classical UBR box found in N-recognin proteins, such as yUBR1, hUBR1, and hUBR2 (Figure 3a). Despite these structural similarities, UBR6 was unable to recognize N-degrons. A comparison of the negatively charged N-degron-binding pockets of N-recognition UBR proteins with the corresponding site in the UBR box of hUBR6 clarified this difference (Figure 3b–e). The UBR boxes of N-recognin UBR proteins had a distinctly negatively charged pocket where type-1 N-degrons bound (Figure 3c–e). In contrast, the UBR6-box lacked a distinctive negative pocket (Figure 3b). The corresponding structural site in hUBR6 was only slightly negative, with a much weaker charge and smaller area, for which sequence analyses provided clear evidence (Figure 2b). The key determinant for the  $\alpha$ -amino group of N-degron was Asp889 in hUBR6 (Asp176—the equivalent residue in yUBR1), which was conserved and generated a small, negatively charged surface at the center. All other specificity determinants for the type-1 N-degrons identified in yUBR1 (residues in parentheses) were not conserved in hUBR6: Thr859 (Asp142), Arg861 (Thr144), Ala892 (Asp179), and Thr894 (Glu181) (Figure 2b). Negatively charged residues in yUBR1 were replaced with short, polar, neutral, or positively charged residues in hUBR6. Therefore, the lack of a sufficiently negatively charged

**FIGURE 2** A monomeric structure of UBR box from hUBR6. (a) A ribbon diagram showing the overall structure of the UBR6-box<sup>824–908</sup>. The N- and C-terminal residues of the model are indicated. Three Zn(II) ions (Zn1, Zn2, and Zn3) are represented by light gray spheres. A bound sulfate ion is also shown. Residues 824–846 (including two additional N-terminal residues, Gly-Ser from the expression vector), 847–885, and 886–904 are colored yellow, magenta, and green, respectively. (b) Sequence alignment of hUBR6 (824–908), yUBR1 (118–194), hUBR1 (97–168), hUBR2 (97–168), hUBR5 (1656–1729), and AtPRT6 (119–189). Orange dots are marked for the conserved zinc-coordinating residues of the sequelogs (Varshavsky 2004). Non-conserved zinc coordination residues, Cys872 of hUBR6, His118 of yUBR1, His166 of hUBR1 (and hUBR2), and His187 of AtPRT6 are marked with green boxes and red arrows. The specificity-determining residues for the N-terminal arginine are marked with blue-filled arrows. The key aspartic residue for the  $\alpha$ -amino group is marked with a green-filled arrow. (c) Three zinc-coordination sites. The Cys868 residue, which bridges two zinc atoms, is shown in red, along with other residues coordinating three zinc ions. The distances between each residue and Zn are shown in angstroms ( $\text{\AA}$ ). (d) Secondary structural elements on the monomeric UBR6-box<sup>824–908</sup> and dimeric UBR6-box<sup>833–904</sup>. The colors of the sequence correspond to those in panel (a). The region for structural determination is marked with brackets. (e) Structural alignment of the monomeric UBR6-box<sup>824–908</sup> (PDB: 7YRB) and the domain-swapped dimeric UBR6-box<sup>833–904</sup> (PDB: 5VMD). The faintly present monomeric and clear dimeric structures are colored the same as those in panel (a). The Zn-coordinating Cys835 residue in the monomeric structure is located at the extended N-terminal region of the monomeric subunit of the dimer structure (left). In the dimeric structure, each monomeric chain is colored dark and light gray, and the superimposed monomeric structure is colored magenta (right). The His<sub>4</sub>-zinc-coordinating site involved in dimerization is indicated by a dotted rectangle. (f) The H848 and H883 residues coordinating zinc ions in the dimer structure are indicated. These residues point in different directions (not involved in zinc coordination) in the monomeric structure compared to the residues in the dimer. (g, h) A detailed view of zinc-binding sites of the monomeric UBR6-box<sup>824–908</sup> (g) and domain-swapped dimeric UBR6-box<sup>833–904</sup>. (h) Note that Cys835 for coordinating Zn1 is missing in the domain-swapped dimer (dotted circle).

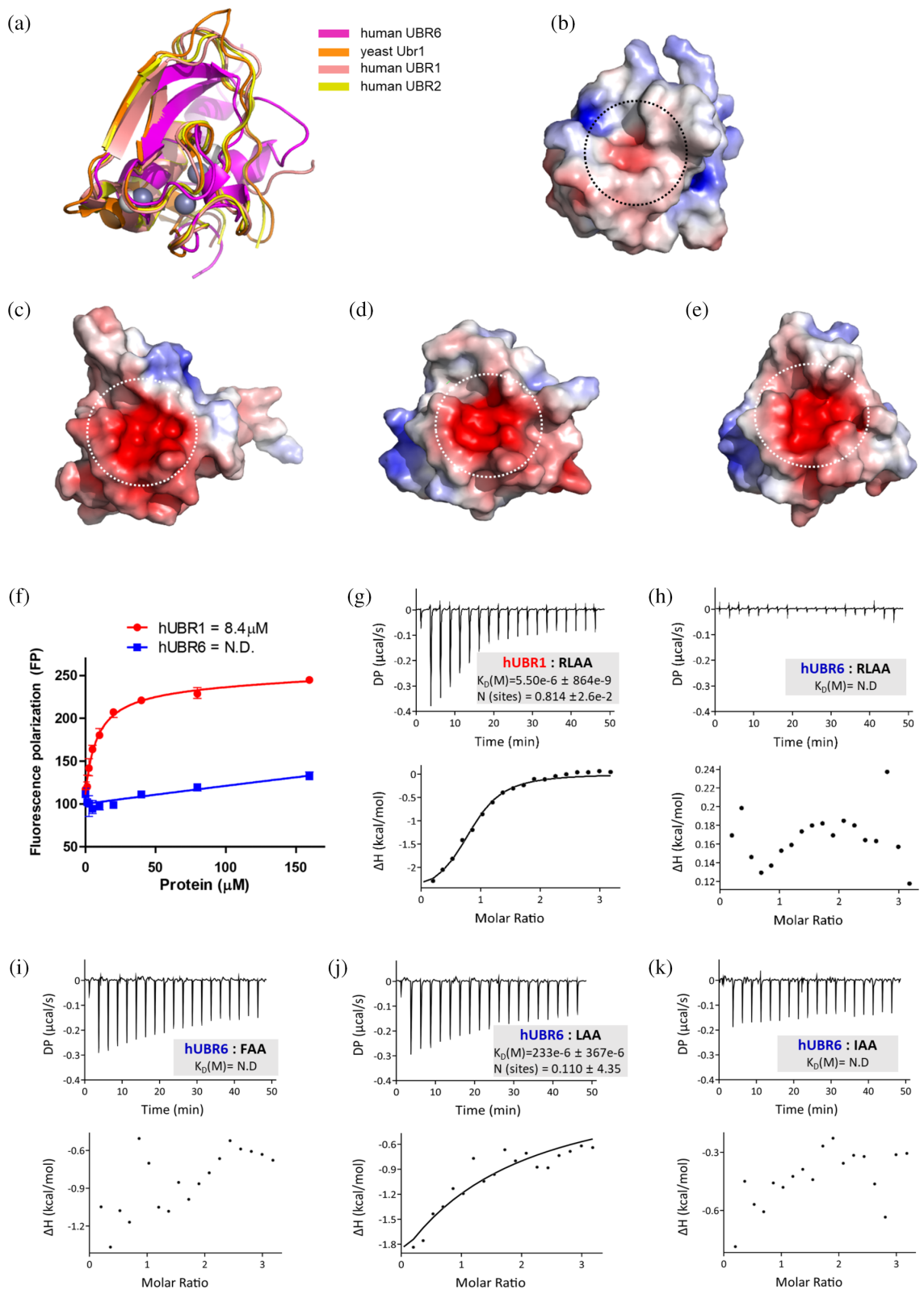


FIGURE 3 Legend on next page.

binding pocket in the hUBR6-box is assumed to be the reason for its inability to function as an N-recognin.

To test the binding affinity of hUBR6 for N-degrons, we performed a fluorescence polarization (FP) binding assay using a FITC-labeled RLAK peptide, which mimics the N-degron substrate (Figure 3f). The UBR box of hUBR1 was also used for comparison. The  $K_D$  values for the functional UBR boxes for the N-degron peptides were in the micromolar range (Tasaki et al. 2009), which was consistent with the current data for hUBR1 (Figure 3f). In contrast, the UBR box of hUBR6 exhibited no measurable binding affinity for the peptide, indicating its inability to interact with the N-degron. These results were further validated by additional isothermal titration calorimetry (ITC) experiments, which confirmed the micromolar  $K_D$  value for the UBR box of hUBR1 to the N-degron peptide and showed no significant binding of the UBR box of hUBR6 to the peptide (Figure 3g,h). Because the electrostatic potential of the putative N-degron binding pocket was not highly negatively charged, we tested the binding affinity of the hUBR6-box to the hydrophobic type-2 N-degron peptides (Figure 3i–k). The  $K_D$  values showed no binding or extremely weak binding of the hydrophobic N-degron substrates.

### 3 | DISCUSSION

The monomeric structure of the hUBR6-box using an N-terminal-extended construct showed a classical UBR domain structure, which was starkly different from the reported dimeric structure (Figure 2). The UBR6-box<sup>824–908</sup> was initiated from the predicted model using AlphaFold2 (Jumper et al. 2021) (Figure S3a). The N-terminal 9-residue-extended construct showed significant differences in protein stability and folding. The longer construct had one more  $\alpha$ -helix at the N-terminal region and remained a monomer. Intriguingly, the model predicted by AlphaFold3 showed a structural discrepancy compared to the high-resolution crystal structure of a shorter construct; however, the revisited crystal structure of a longer construct matched the predicted structure (Figure 2a). Therefore, the AlphaFold3 prediction was deemed useful for re-investigating the experimental structure, which revealed an unexpected folding or structure compared to what

was originally anticipated. However, this dimer structure should not be regarded as incorrect. The zinc coordination in both structures was almost identical, and the domain-swapped dimer mimicked the monomer structure. Thus, the possibility that both structures coexist under physiological conditions in different equilibrium states cannot be ruled out.

In addition to the new monomeric structure, we explained why hUBR6 did not function as an N-recognin. In contrast to the interpretation using the dimeric structure, the monomeric structure of the UBR6-box showed a distinct negatively charged pocket, although all of these UBR boxes shared the classical UBR box fold. This electrostatic surface difference explains why UBR6, unlike UBR1 and UBR2, does not bind the type-1 N-degron. The UBR box of UBR4 possesses the binding affinity to the type-2 N-degron (Jeong et al. 2023). However, our UBR6-box showed no binding or extremely weak binding (Figure 3i–k). Therefore, hUBR6 does not function as an N-recognition protein, which is consistent with the fact that the substrates of hUBR6 mediated by the UBR box are not yet clearly identified. To comprehensively understand the function of hUBR6, the whole SCF complex of the entire hUBR6 with SKP1-CUL1-RBX1 remains an important objective for future research.

### 4 | MATERIALS AND METHODS

#### 4.1 | Cloning

The UBR box domains (residues 824–908 and 833–908) of human UBR6 were amplified using PCR from codon-optimized gBlock gene fragments (Integrated DNA Technologies). The DNA fragments were cloned into the BamHI and Xhol restriction sites of the pRSF vector containing N-terminal hexa-histidines and a small ubiquitin-like modifier (SUMO) tag, followed by a TEV cleavage site. Both plasmids were transformed into *Escherichia coli* BL21 (DE3) cells.

#### 4.2 | Protein expression and purification

The transformed cells were grown in Luria Broth media containing kanamycin (50  $\mu$ g/mL) at 37°C until OD<sub>600nm</sub>

**FIGURE 3** Comparison of UBR boxes from hUBR6, yUBR1, hUBR1, and hUBR2. (a) Structural alignment of hUBR6 (magenta; PDB: 7YRB), yUBR1 (orange; PDB: 3NIT), hUBR1 (salmon; PDB: 3NY1), and hUBR2 (yellow; PDB: 3NY2). (b–e) Electrostatic potential surfaces of UBR box from hUBR6 (b), yUBR1 (c), hUBR1 (d), and hUBR2 (e). Negatively and positively charged surfaces are shown in red and blue, respectively. A dotted circle indicates the region corresponding to the negatively charged pocket of N-recognin. (f) FP assays using FITC-labeled RLAK-peptide against increasing concentrations of hUBR1 (red line) and hUBR6 (blue line); the error bars represent standard error of the mean of more than three independent experiments; N.D., not determined. (g–k) ITC was performed to measure the binding affinity of the RLAA-peptide to the hUBR1-box (g) and hUBR6-box (h). The binding affinity between hUBR6-box and the type-2 N-degron peptides, FAA (i), LAA (j), and IAA (k) was also measured. Note that the standard deviation of the  $K_D$  value for LAA affinity is too large for convincing data. The top panel shows the raw ITC thermogram and the bottom panel presents the corresponding binding isotherm with fitted curves.

reached 0.6. The expression of N-terminal hexa-histidine-SUMO-tagged hUBR6 824–908 or 833–908 protein was induced by a final concentration of 0.5 mM isopropyl  $\beta$ -D-1-thiogalactopyranoside and 700  $\mu$ M of ZnSO<sub>4</sub> at 18°C for 24 h. Cells were harvested by centrifugation at 6000g using a Beckman J-20 machine for 20 min. Harvested cells were resuspended in His-binding buffer (50 mM Tris-HCl [pH 8.0], 200 mM NaCl, and 1 mM Tris [2-carboxyethyl] phosphine [TCEP]). Phenylmethyl sulfonyl fluoride was added to a concentration of 1.0 mM, and a complete protease inhibitor cocktail (Roche) was added to the resuspended cells to inhibit protease activity. The cells were sonicated, and insoluble materials were removed by centrifugation at 35,000g for 2 h. The supernatant was loaded onto a HisTrap HP column (5 mL; Cytiva) and eluted by gradient purification using His elution buffer (50 mM Tris-HCl [pH 8.0], 100 mM NaCl, 1.0 mM TCEP, and 0.5M imidazole). The eluent was diluted with a 5-fold volume by mixing with Q binding buffer (50 mM Tris-HCl [pH 8.0], 1.0 mM TCEP, and 10  $\mu$ M ZnCl<sub>2</sub>) and then loaded into a HiTrap Q HP column (5 mL; Cytiva). The protein was eluted by gradient purification using Q elution buffer (50 mM Tris-HCl [pH 8.0], 1.0M NaCl, 1.0 mM TCEP, and 10  $\mu$ M ZnCl<sub>2</sub>). The eluate fractions containing the target protein were collected and treated with TEV protease for 10 h at 22°C. To remove the hexa-histidine-tagged TEV protease and the cleaved hexa-histidine-SUMO tag from the target protein, a second His affinity chromatographic step was performed. The loading through was concentrated using ultrafiltration (Amicon Ultra 3K NMWL, Millipore). The concentrated protein was loaded onto a HiLoad 16/600 Superdex 75 pg (Cytiva) column equilibrated with gel filtration buffer (25 mM Tris-HCl [pH 7.5], 100 mM NaCl, and 1 mM TCEP). The monomer fractions of the eluate were concentrated, and the final concentration was determined using the Bradford assay. Purity was determined by SDS-PAGE, followed by staining with Coomassie blue for protein detection.

### 4.3 | SEC-MALS

Size-exclusion chromatography coupled with multi-angle light scattering (SEC-MALS) was performed to confirm the oligomeric state of hUBR6-box<sup>824–908</sup>. Purified proteins were concentrated by ultrafiltration (Amicon® Ultra 3K NMWL, Millipore) to 10 mg/mL and were loaded onto an S75 Increase 10/300 GL column (29148721; Cytiva) pre-equilibrated with gel filtration buffer. MALS data were collected using a miniDAWN (Wyatt Technology, Santa Barbara, CA). Before the experiment, 4 mg of ovalbumin (Sigma-Aldrich; A5503) was injected into the column for normalization. The theoretical molecular mass and molar extinction coefficient at 280 nm of the UBR6-UBR box monomer (residues

824–908 with an N-terminal GS sequence remaining after TEV protease cleavage) were 9959.06 g/mol and 5960 M<sup>-1</sup> cm<sup>-1</sup>, respectively, accounting for the presence of three Zn(II) ions. The theoretical molecular mass and molar extinction coefficient at 280 nm of the UBR6-UBR box dimer (residues 824–908 with an N-terminal GS sequence remaining after TEV protease cleavage) were 19983.5 g/mol and 11,920 M<sup>-1</sup> cm<sup>-1</sup>, respectively, accounting for the presence of seven Zn(II) ions. Data analysis was performed using the ASTRA 8 software (Wyatt Technology).

### 4.4 | Crystallization and data collection

To find the crystallization conditions of the UBR6-box<sup>824–908</sup>, the monomer fraction of the size-exclusion chromatography eluent was concentrated to 7, 12, and 19 mg/mL. A Gryphon machine (Art Robbins Instrument) was used for the initial crystallization screening. Equal volumes of protein and reservoir were mixed for crystallization using the sitting-drop vapor diffusion method in 96-well plates. The initial crystal of the hUBR6-box monomer was grown at 22°C under conditions of 0.1M HEPES (pH 7.5), 2.0M ammonium sulfate, and 2% (v/v) polyethylene glycol 400 (PEG400). Crystal quality was improved using a combination of 2.0–2.2M ammonium sulfate and 1%–3% (v/v) PEG400. The crystals were flash-frozen in liquid nitrogen with 20% (v/v) glycerol added to the original solution as a cryoprotectant. Datasets for the UBR box from hUBR6 were collected using the 5C beamline at the Pohang Accelerator Laboratory in South Korea. The diffraction data were indexed, integrated, and scaled using HKL2000 (Otwinowski and Minor 1997). The data collection statistics for the hUBR6-box<sup>824–908</sup> crystals are summarized in Table S1.

### 4.5 | Structure determination and refinement

Because the hUBR6-box<sup>824–908</sup> is a zinc finger domain, the phases were obtained using MAD data: zinc absorption peak, edge, and remote (Table S1). Model building was performed using COOT (Emsley 2017). Refinement was performed using PHENIX (Adams et al. 2010). The refinement statistics are summarized in Table S1. All structural figures were drawn using PyMOL (Mooers and Brown 2021) (<http://www.pymol.org/>).

### 4.6 | Sequence alignment and phylogenetic analysis

The sequences of hUBR6 (824–908), yUBR1 (118–194), hUBR1 (97–168), and hUBR2 (97–168) were

aligned using Clustal Omega (Sievers et al. 2011), and similarities were identified using ESPript 3.0 (Robert and Gouet 2014). The phylogenetic trees of seven mammalian UBR family proteins (hUBR1 97–168, hUBR2 97–168, hUBR3 118–189, hUBR4 1656–1729, hUBR5 1177–1245, hUBR6 833–904, and hUBR7 44–116) were analyzed and drawn using Clustal Omega.

## 4.7 | Fluorescence polarization assay

The binding affinities of UBR boxes from hUBR1 (residues 97–167) and hUBR6 (residues 824–908) to the peptide were determined using FP techniques. FITC-labeled RLAK-peptide purchased from Peprion Inc. was dissolved to a concentration of 1 mM in assay buffer (50 mM HEPES-NaOH [pH 7.5], 100 mM NaCl, and 1 mM TCEP) and sequentially diluted with the buffer to 100 nM in each reaction well. Purified His-SUMO-UBR boxes from hUBR1 and hUBR6 were also serially diluted in the buffer and mixed into each reaction well at a concentration of 1–160 μM. Fluorescence measurements to detect the change in light polarization of the FITC-labeled peptide were performed in a 384-well plate on a Corning black plate reader at excitation and emission wavelengths of 485 and 535 nm, respectively. A nonlinear graph of the UBR box concentration-dependent polarization was plotted using GraphPad Prism 10 software.

## 4.8 | Isothermal titration calorimetry

The same assay buffer was used for the FP assay and ITC experiments. His-SUMO-UBR boxes from hUBR1 (97–167) and hUBR6 (824–908) were diluted to a concentration of 50 μM in ITC buffer, and the N-degron peptides (RLAA, FAA, LAA, and IAA) were dissolved in the same buffers at a concentration of 800 μM. The experiment was performed at 25°C using a Microcal PEAQ-ITC instrument (Malvern Instruments Inc.). Each peptide was injected 19 times (2 μL each) into 280 μL samples of each protein. The experimental data were analyzed using an embedded analysis software package provided by the instrument.

## AUTHOR CONTRIBUTIONS

**Bokyung Kim:** Conceptualization; data curation; visualization; validation; writing – review and editing; writing – original draft. **Sohae Lee:** Conceptualization; data curation; validation; writing – original draft; visualization; writing – review and editing. **Bong Heon Kim:** Supervision; validation; data curation; methodology. **Leehyeon Kim:** Conceptualization; project administration; resources. **Hyun Kyu Song:** Conceptualization; writing – original draft; writing – review and editing;

supervision; formal analysis; funding acquisition; project administration; resources; visualization.

## ACKNOWLEDGMENTS

We thank the staff at Beamline 5C of the Pohang Accelerator Laboratory, Korea. This study was partly supported by the International Collaborative Research Program of the Institute for Protein Research at Osaka University (ICR-23-05). Diffraction data were collected at the Osaka University beamline BL44XU at SPring-8 (Harima, Japan) (Proposal No. 2023A6873). This work was also supported by grants from the National Research Foundation of Korea (RS-2020-NR049540, RS-2021-NR056525, RS-2021-NR056577, and RS-2022-NR067411) from the Korean government, and in part by a Korea University Grant.

## CONFLICT OF INTEREST STATEMENT

The authors declare no conflicts of interest.

## DATA AVAILABILITY STATEMENT

The data that support the findings of this study are openly available in Protein Data Bank at <https://www.rcsb.org/>, reference number 7YRB.

## ORCID

Hyun Kyu Song  <https://orcid.org/0000-0001-5684-4059>

## REFERENCES

- Abbas T, Keaton M, Dutta A. Regulation of TGF-beta signaling, exit from the cell cycle, and cellular migration through cullin cross-regulation: SCF-FBXO11 turns off CRL4-Cdt2. *Cell Cycle*. 2013a;12:2175–82.
- Abbas T, Mueller AC, Shibata E, Keaton M, Rossi M, Dutta A. CRL1-FBXO11 promotes Cdt2 ubiquitylation and degradation and regulates Pr-Set7/Set8-mediated cellular migration. *Mol Cell*. 2013b;49:1147–58.
- Abida WM, Nikolaev A, Zhao W, Zhang W, Gu W. FBXO11 promotes the Neddylation of p53 and inhibits its transcriptional activity. *J Biol Chem*. 2007;282:1797–804.
- Abramson J, Adler J, Dunger J, Evans R, Green T, Pritzel A, et al. Accurate structure prediction of biomolecular interactions with AlphaFold 3. *Nature*. 2024;630:493–500.
- Adams PD, Afonine PV, Bunkoczi G, Chen VB, Davis IW, Echols N, et al. PHENIX: a comprehensive Python-based system for macromolecular structure solution. *Acta Crystallogr D Biol Crystallogr*. 2010;66:213–21.
- Bachmair A, Finley D, Varshavsky A. In vivo half-life of a protein is a function of its amino-terminal residue. *Science*. 1986;234: 179–86.
- Bartel B, Wunning I, Varshavsky A. The recognition component of the N-end rule pathway. *EMBO J*. 1990;9:3179–89.
- Choi WS, Jeong BC, Joo YJ, Lee MR, Kim J, Eck MJ, et al. Structural basis for the recognition of N-end rule substrates by the UBR box of ubiquitin ligases. *Nat Struct Mol Biol*. 2010;17:1175–81.
- Duan S, Cermak L, Pagan JK, Rossi M, Martinengo C, di Celle PF, et al. FBXO11 targets BCL6 for degradation and is inactivated in diffuse large B-cell lymphomas. *Nature*. 2012;481:90–3.
- Emsley P. Tools for ligand validation in Coot. *Acta Crystallogr D Struct Biol*. 2017;73:203–10.

- Finley D. Recognition and processing of ubiquitin-protein conjugates by the proteasome. *Annu Rev Biochem*. 2009;78:477–513.
- Hodakova Z, Grishkovskaya I, Brunner HL, Bolhuis DL, Belacic K, Schleifer A, et al. Cryo-EM structure of the chain-elongating E3 ubiquitin ligase UBR5. *EMBO J*. 2023;42:e113348.
- Horn M, Geisen C, Cermak L, Becker B, Nakamura S, Klein C, et al. DRE-1/FBXO11-dependent degradation of BLMP-1/BLIMP-1 governs *C. elegans* developmental timing and maturation. *Dev Cell*. 2014;28:697–710.
- Jackson PK, Eldridge AG. The SCF ubiquitin ligase: an extended look. *Mol Cell*. 2002;9:923–5.
- Jeong DE, Lee HS, Ku B, Kim CH, Kim SJ, Shin HC. Insights into the recognition mechanism in the UBR box of UBR4 for its specific substrates. *Commun Biol*. 2023;6:1214.
- Jin J, Cardozo T, Lovering RC, Elledge SJ, Pagano M, Harper JW. Systematic analysis and nomenclature of mammalian F-box proteins. *Genes Dev*. 2004;18:2573–80.
- Juniper J, Evans R, Pritzel A, Green T, Figurnov M, Ronneberger O, et al. Highly accurate protein structure prediction with AlphaFold. *Nature*. 2021;596:583–9.
- Kim BH, Kwon DH, Kim L, Yang WS, Song HK. In vitro production of N-degron fused proteins and its application. *Methods Enzymol*. 2023;686:99–123.
- Kim L, Heo J, Kwon DH, Shin JS, Jang SH, Park ZY, et al. Structural basis for the N-degron specificity of ClpS1 from *Arabidopsis thaliana*. *Protein Sci*. 2021;30:700–8.
- Kim L, Kwon DH, Heo J, Park MR, Song HK. Use of the LC3B-fusion technique for biochemical and structural studies of proteins involved in the N-degron pathway. *J Biol Chem*. 2020;295:2590–600.
- Kipreos ET, Pagano M. The F-box protein family. *Genome Biol*. 2000;1:3002.
- Matta-Camacho E, Kozlov G, Li FF, Gehring K. Structural basis of substrate recognition and specificity in the N-end rule pathway. *Nat Struct Mol Biol*. 2010;17:1182–7.
- Mooers BHM, Brown ME. Templates for writing PyMOL scripts. *Protein Sci*. 2021;30:262–9.
- Munoz-Escobar J, Kozlov G, Gehring K. Crystal structure of the UBR-box from UBR6/FBXO11 reveals domain swapping mediated by zinc binding. *Protein Sci*. 2017;26:2092–7.
- Munoz-Escobar J, Matta-Camacho E, Cho C, Kozlov G, Gehring K. Bound waters mediate binding of diverse substrates to a ubiquitin ligase. *Structure*. 2017b;25:719–729.e3.
- Otwinowski Z, Minor W. Processing of X-ray diffraction data collected in oscillation mode. *Methods Enzymol*. 1997;276:307–26.
- Pan M, Zheng Q, Wang T, Liang L, Mao J, Zuo C, et al. Structural insights into Ubr1-mediated N-degron polyubiquitination. *Nature*. 2021;600:334–8.
- Robert X, Gouet P. Deciphering key features in protein structures with the new ENDscript server. *Nucleic Acids Res*. 2014;42:W320–4.
- Rossi M, Duan S, Jeong YT, Horn M, Saraf A, Florens L, et al. Regulation of the CRL4(Cdt2) ubiquitin ligase and cell-cycle exit by the SCF(Fbxo11) ubiquitin ligase. *Mol Cell*. 2013;49:1159–66.
- Schrader EK, Harstad KG, Matouschek A. Targeting proteins for degradation. *Nat Chem Biol*. 2009;5:815–22.
- Sievers F, Wilm A, Dineen D, Gibson TJ, Karplus K, Li W, et al. Fast, scalable generation of high-quality protein multiple sequence alignments using Clustal Omega. *Mol Syst Biol*. 2011;7:539.
- Skaar JR, Pagan JK, Pagano M. Mechanisms and function of substrate recruitment by F-box proteins. *Nat Rev Mol Cell Biol*. 2013;14:369–81.
- Sriram SM, Kim BY, Kwon YT. The N-end rule pathway: emerging functions and molecular principles of substrate recognition. *Nat Rev Mol Cell Biol*. 2011;12:735–47.
- Tasaki T, Kwon YT. The mammalian N-end rule pathway: new insights into its components and physiological roles. *Trends Biochem Sci*. 2007;32:520–8.
- Tasaki T, Mulder LC, Iwamatsu A, Lee MJ, Davydov IV, Varshavsky A, et al. A family of mammalian E3 ubiquitin ligases that contain the UBR box motif and recognize N-degrons. *Mol Cell Biol*. 2005;25:7120–36.
- Tasaki T, Sriram SM, Park KS, Kwon YT. The N-end rule pathway. *Annu Rev Biochem*. 2012;81:261–89.
- Tasaki T, Zakrzewska A, Dudgeon DD, Jiang Y, Lazo JS, Kwon YT. The substrate recognition domains of the N-end rule pathway. *J Biol Chem*. 2009;284:1884–95.
- Tsai JM, Aguirre JD, Li YD, Brown J, Focht V, Kater L, et al. UBR5 forms ligand-dependent complexes on chromatin to regulate nuclear hormone receptor stability. *Mol Cell*. 2023;83(15):2753–2767.e10. <https://doi.org/10.1016/j.molcel.2023.06.028>
- Varshavsky A. The N-end rule: functions, mysteries, uses. *Proc Natl Acad Sci U S A*. 1996;93:12142–9.
- Varshavsky A. “Spalog” and “sequelog”: neutral terms for spatial and sequence similarity. *Curr Biol*. 2004;14:R181–3.
- Varshavsky A. The N-end rule pathway and regulation by proteolysis. *Protein Sci*. 2011;20:1298–345.
- Varshavsky A. N-degron and C-degron pathways of protein degradation. *Proc Natl Acad Sci U S A*. 2019;116:358–66.
- Varshavsky A. N-degron pathways. *Proc Natl Acad Sci U S A*. 2024;121:e2408697121.
- Wang F, He Q, Zhan W, Yu Z, Finkin-Groner E, Ma X, et al. Structure of the human UBR5 E3 ubiquitin ligase. *Structure*. 2023;31:541–552.e4.

## SUPPORTING INFORMATION

Additional supporting information can be found online in the Supporting Information section at the end of this article.

**How to cite this article:** Kim B, Lee S, Kim BH, Kim L, Song HK. Revisiting the structure of UBR box from human UBR6. *Protein Science*. 2025;34(4):e70092. <https://doi.org/10.1002/pro.70092>